P3.7 ATMOSPHERIC TURBULENCE EFFECTS ON NEAR-GROUND WAKE VORTEX DEMISE

Hadi S. Wassaf, Amir Tabrizi, Frank Y. Wang, and Melanie Soares
US DOT RITA John A. Volpe National Transportation Systems Center
Cambridge MA

1. INTRODUCTION

The Federal Aviation Administration (FAA) and National Aeronautics and Space Administration (NASA) have been working jointly on a phased approach to implement wake avoidance solutions designed to safely reduce wake turbulence separation standards in the United States (Bryant et. al. 2007 and Lang et. al. 2007). Currently the FAA-NASA partnership is pursuing mid-term solutions characterized as wind-dependent procedures for Closely Spaced Parallel Runway (CSPR) airports involving Heavy and B757 category aircraft (Lang et. al. 2007). The program has entered a field data collection phase for, amongst other things, wind and vortices from departing aircraft as the necessary building blocks to construct a comprehensive safety assessment of the new procedures.

From the wake vortex measurement perspective, particular emphasis has been placed on vortices generated at around two initial vortex spacing altitudes otherwise commonly known as the near-ground-effect (NGE) regime (Robins and Delisi, 2001). The reason is twofold: Firstly, the near the ground region is considered the more critical area in the event of a wake encounter as the aircraft would have less altitude to recover from an upset. Secondly, in the NGE regime, general knowledge of wake transport and demise, therefore the reliability of the wake models, are less matured compared to their counterparts for out-of-ground effect (OGE) regime.

In addition, because of interest in CSPR operations, the downwind vortex (i.e., the vortex that would travel towards the adjacent runway under zero or light crosswind component (Dee and Nicholas, 1968 and Köpp, 1999)) dynamics merit an in-depth investigation. For this purpose, wake, wind and atmospheric turbulence measurements near the ground were made concurrently. The current paper is to examine the general question of downwind vortex demise and the mechanisms involved using the data collected to support mid-term solutions.

The current paper is a continuation of an earlier exploratory effort (Mackey et. al. 2007) to examine the demise time of the vortices versus eddy dissipation rate (EDR) near the ground. However, the present work distinguishes itself from the aforementioned work (Mackey, et. al. 2007) in that wake and turbulence data were collected simultaneously instead of in two separate phases. As such, a more direct correlation of the EDR and wake dynamics has been made. Secondly, wake vortex data were examined from both the perspectives of circulation decay as well as breakup of as a function of EDR. It is noteworthy that although the role of turbulence is shown to dominate the OGE wake decay process (Greene, 1986 and Sarpkaya et. al. 2001), its role for vortex decay near the ground is not universally agreed upon (Proctor, et. al. 2000, Spalart, et. al. 2001, Burnham and Hallock, 2005, Frech, 2007, Holzäpfel and Meiko, 2007).

2. TEST DESCRIPTION

The atmospheric and wake data analyzed and presented in this paper are collected at the George Bush Intercontinental Airport (IAH) in Houston, Texas. The airport diagram along with sensors' positions and coordinate system conventions are shown in Figure 1.

A WindTracer® pulsed LIDAR manufactured by Lockheed Martin Coherent Technologies (formerly Coherent Technologies, Inc.) was positioned at x=2452 ft and y=1390 ft away from Runway 33L threshold and configured to scan perpendicular to the path of airplanes departing from both 15L and 15R. This LIDAR was used to determine lateral (x) and vertical (z) positions of departure wake vortices and to provide estimates of their strength

in terms of total circulation. A Campbell Scientific® CSAT3 sonic anemometers sampling at 20 Hz was mounted on a 50 ft pole positioned approximately at x=-1350 ft y=-1200 ft relative to Runway 33L threshold as shown in Figure 1. The sonic anemometer is oriented such that it faces headwind during runway 15 departures to minimize flow contamination from the sensor's supporting structures. The CSAT3 is used to measure EDR near the surface for the purpose of quantifying near-ground turbulence effects on the lifetimes of wakes generated in the NGE regime.

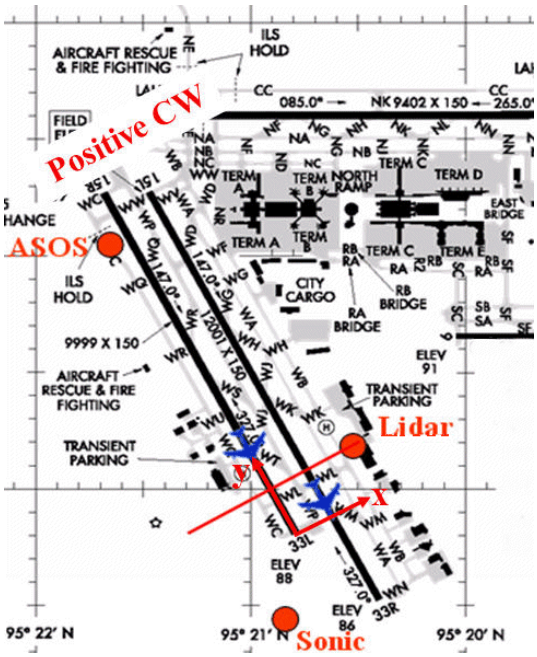

Figure 1: Airport diagram with sensors locations. The coordinate system convention used throughout the paper is also shown.

Although the sonic anemometer provides headwind and crosswind measurements relative to the runways, the official surface wind source from the airport is used instead to better integrate the results to gain potential operational insights. Therefore, wind magnitude and direction from the Automated Surface Observing System (ASOS) was used to investigate the surface EDR dependence on total wind measured by a standard airport system. ASOS measures the horizontal wind at 10 meters height (32.8 ft) and outputs the data at a rate of once a minute. Both the sonic and ASOS locations are also shown in Figure 1.

3. DATA DESCRIPTION

The wake and EDR data collected by LIDAR and sonic anemometer, respectively, from 08/23/2007 to 10/15/2007 have been used for the analyses presented herein. For each aircraft type, only the wakes generated in NGE (defined here as initial vortex generation altitudes two times that of the theoretical initial vortex separation $b_o \pm 0.3 * b_o$ based on the elliptic wing loading) regime are kept for subsequent analyses. The resulting number of wake tracks, binned by aircraft type, is shown in Table 1.

AC Type	Count
B733	632
B735	494
B737	373
B738	613
B739	64
B752	65
B753	115
B762	30
B764	1
B772	2

Table 1: Counts of wake tracks used in the analysis segregated by airplane type.

The EDR results are derived from the three-component wind measurements using the spectral method (Perras and Dasey, 2000). First, each time series (representing a wind component) is subdivided into 30 min intervals. The wind reference coordinate system is subsequently rotated so that positive Ux is in the direction of the mean wind, Uy is the perpendicular to Ux in the horizontal plane, and z is such that <Ux,Uy,Uz> form a right-hand orthonormal coordinate system (Uz is nearly vertical unless the vertical wind component is unusually high). The wave-number Power Spectral Density (PSD) is then calculated for each wind component, and the inertial subrange is found in scale by detecting the linear region of each of the PSDs that has a slope satisfying: Slope=-5/3 (within a prescribed tolerance) on a log-log scale. It may be noteworthy to indicate that the range of eddy size included in the EDR calculation is of the order of those that would exit in wake vortices. The choice of EDR as a possible mean to correlate the general wake dynamics is hence warranted.

For each LIDAR scan, averaged spectra per range gate are computed and stored for subsequent post processing. The LIDAR data

processing utilizes a maximum likelihood method (Hannon, et. al. 1997) applied in the spectral domain to detect and estimate the vortex parameters. The Likelihood is calculated for every hypothesized vortex position, strength, and core size based on the Burnham-Hallock vortex model (Gerz, et. al. 2002), The likelihood ratio is used to test the vortex not present hypothesis H_0 against the vortex present alternative H_1. In the case that a vortex is detected, its parameters are those that maximize the log-likelihood. This approach is cast in the form of matched filters for faster computation. For the scan configuration deployed at IAH, vortex data have a typical time resolution of 8.5 seconds.

A series of data quality control steps are employed in the selection of both sonic and LIDAR data. The sonic data are screened for consistency and validity by monitoring data skips and performing tests on the spectral shape of all three wind components. Also, the difference in EDRs calculated from the three components are required to be within a predefined uncertainty bound. In addition, the post-processing of the LIDAR data included a tight tolerance between the initial wake detection and aircraft passage times. In order to account for the greater maneuverability of the downwind vortex transport near the ground, parameters in the Kalman filter tracker used as part of the LIDAR processing had been relaxed. Also a wake must be tracked at least 20 seconds to be considered valid, and a track sorting algorithm was also used to re-combine individual wake tracks that should have belong together owning to the non-monotonic nature of the signal to noise ratio often observed in wake measurements. Finally, the vortices that have reached the edge of the post-processing spatial domain are removed to avoid adverse effects on the analysis.

EDR (ε), wake age (T), and wake circulation (Γ) data are subsequently transformed to non-dimensional quantities denoted by ε^*, T^*, and Γ^* respectively according to the equations below:

$$\varepsilon^* = \frac{(\varepsilon . b_o)^{1/3}}{V_o} \qquad (1)$$

$$T^* = \frac{T . b_o}{V_o} \qquad (2)$$

$$\Gamma^* = \frac{\Gamma}{\Gamma_o} \qquad (3)$$

where b_o, Γ_o, and V_o represent the initial vortex spacing, circulation and descend velocity respectively and are calculated using the equations below. $T_o = b_o / V_o$ is the time needed for the vortex pair to descend a distance of b_o.

$$b_o = \frac{\pi}{4} . s \qquad (4)$$

$$\Gamma_o = \frac{g.(0.9.W_T)}{\rho_o . V_{TAS} . b_o} \qquad (5)$$

$$V_o = \frac{\Gamma_o}{2.\pi . b_o} \qquad (6)$$

where s, W_T, and V_{TAS} are the airplane's wingspan, maximum takeoff mass, and true air speed respectively. The nominal weight of the aircraft is assumed to be 90 percent of the maximum takeoff weight, and the true air speed is assumed to be 10 knots greater than the landing speed. All other nominal aircraft parameters are taken from Jane's all the World's Aircraft (Jackson, various volumes).

Although the aforementioned normalization is developed for OGE wake dynamics, it is used for the subsequent NGE analyses nevertheless, for the purpose of comparing the data trends with a model developed using OGE data. Also, using this normalization, all wake (not just those from Heavy and/or B757) and turbulence data can be treated as a single large data set.

4. ANALYSES AND RESULTS

As indicated earlier, the present paper is focused on the analyses of downwind vortices. These are defined as vortices with induced ground motion in the same direction as the crosswind. In all of the following plots the bounds are the bootstrapped 90% confidence intervals on the estimate of the median.

The overall motivation of the investigation has been inspired by the observation that regardless of departure or arrival vortices, a universal trend of wake vortex demise time near the ground has an inverse relationship with surface wind (Mackey, et. al. 2007). An example of this phenomenon, taken from the NGE dataset for B733 from IAH, is shown in Figure 2.

When the entire NGE dataset summarized in Table 1 is non-dimensionalized, as expected, the dimensionless wake demise time and wind speed again form the same inverse relationship and is shown as Figure 3. Although wind is a useful parameter for providing operational insights of the data, the underlying mechanism however is more likely to be related to aspects of turbulence in the vortex-ground interaction. The role of the turbulence, drawing from the OGE experience, has been both to accelerate circulation decay as well as promote vortex instability to break up wakes.

Since quicker wake demise under high wind implies either faster overall circulation decay or accelerated time to reach a catastrophic state, such as Crow linking with the ground, it is very likely that the observation is due to an increase in turbulence under high wind, as the analysis will demonstrate. Figure 4 shows that surface EDR increases by about two orders of magnitude as the mean wind goes from 1 to 14 knots. The trend observed in Figure 4 is not entirely unexpected as measurements are made near the surface, thus well within the boundary layer.

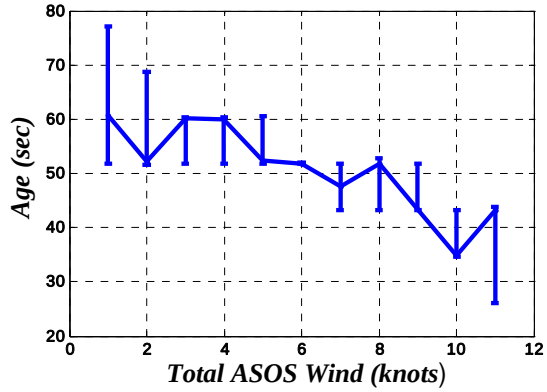

Figure 2: NGE Wake demise time for B733 observed in the IAH database. An inverse relationship between wake demise time and surface wind is noted. The vertical bars indicate the 90% confidence intervals on the median.

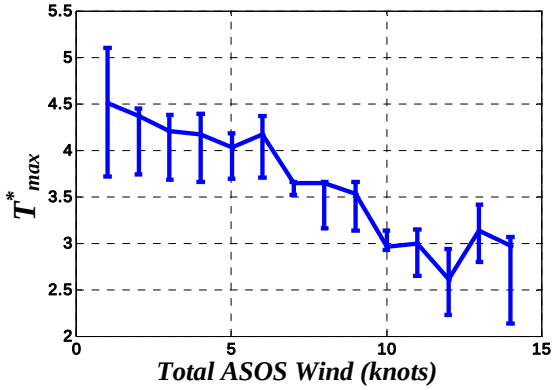

Figure 3: Non-dimensional median wake age as a function of median ASOS wind magnitude. The vertical bars indicate the 90% confidence intervals on the median.

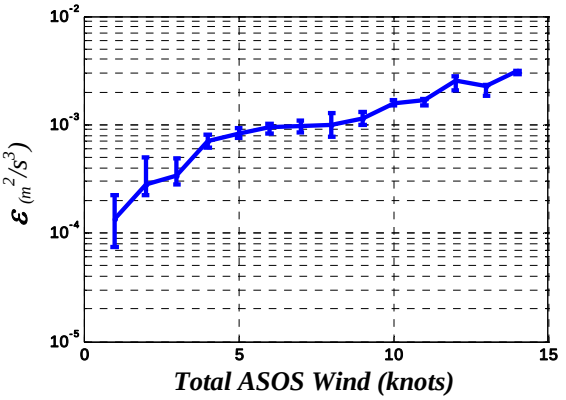

Figure 4: EDR versus total ASOS wind. EDR is calculated from high-frequency (20 Hz) sonic data.

To examine the demise time due to instability, the final wake age is compared with the theoretically calculated time to reach a catastrophic state. First, a correlation between non-dimensional wake age (T^*_{Max}) and non-dimensional EDR (ε^*) is made and shown in Figure 5.

The blue curve shows the median T^*_{Max} as measured by LIDAR (along with 90% confidence intervals) versus the ε^* obtained from the sonic anemometer. Next, theoretical time for vortices to reach a catastrophic state such as Crow linking is calculated from the model of Sarpkaya (2001). Although the model was developed from OGE arrival wake data, field observation has shown that Crow linking also exists for vortices generated near the ground (Dee and Nicholas 1968, and Proctor et. al. 2000) and simulation (Proctor, et. al.

2000) also suggested that the similar instability triggered vortex catastrophic state may also be due to ambient turbulence. The application of the model by Sarpkaya (2001) in the present study further implicitly assumes that once the vortex pairs have rolled up, the downstream evolution is governed by the same physics, so that models developed from arrival data can be used in departure applications (Mackey et. al. 2007).

For the available range of ε^* in the present study, it is noted that the observed T^*_{Max} is similar to that of predicted by the Sarpkaya model with an average upward bias of about one non-dimensional time. This observation is taken as a circumstantial evidence that, on average, NGE wakes survive no longer than one dimensional time beyond the onset of the catastrophic state such as vortex linking and bursting. It also further supports the expectation that EDR has an influence on the wake demise time near the ground.

It is noteworthy that most of the data in the current study are considered to be of low to moderate turbulence ($\varepsilon^*<0.2$) as classified by Sarpkaya (2001). Extension of the investigation into high turbulence range would be of great interest operationally.

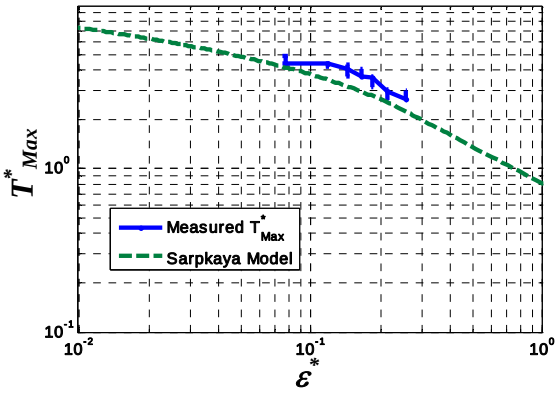

Figure 5: Non-dimensional wake age (for wakes generated in NGE) versus non-dimensional EDR (ε^*) superimposed on the Sarpkaya model of the time for wakes to get into a catastrophic state.

Next, the circulation decay near the ground under different turbulence conditions is investigated. First, the non-dimensional circulation values Γ^* for the wake data are computed and then grouped into non-dimensional time bins $\Gamma^*_{T^*}$ with $T^*=0,1,2,3,4$ and 5. Each group $\Gamma^*_{T^*}$ (containing non-dimensional circulations at a particular value T^*) is further sub-divided into bins based on the corresponding value of ε^*. Finally, the median of the non-dimensional circulation along with the 90% confidence interval on the median are calculated for each corresponding ε^* bin to form $\Gamma^*_{T^*}(\varepsilon^*)$. The result is a non-dimensional circulation curve as a function of ε^* for each fixed T* as shown in Figure 6. It is important to note that each median curve $\Gamma^*_{T^*}(\varepsilon^*)$ is normalized by $\Gamma^*_0(\varepsilon^*)$ to center the initial non-dimensional circulation to unity under all EDR conditions. As the NGE circulation decay behavior as well as the sensitivity to EDR compared to their OGE counterparts are of great interest, in the absence of available OGE data, the corresponding OGE trends are generated using the EDR based wake model from Sarpkaya (2001, and Perras and Dasey, 2000). The aforementioned NGE $\Gamma^*_{T^*}(\varepsilon^*)$ data and calculated OGE trends are presented in Figure 6. In the OGE calculations, the stratification term in the circulation decay model has been disabled. Since the stratification term is of secondary influence, the assumption is not likely to alter the qualitative nature of the comparison between OGE and NGE regimes.

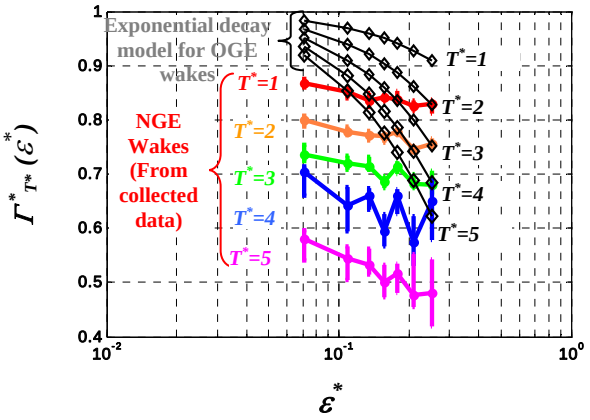

Figure 6: Dependence of Non-dimensional circulation $\Gamma^*_{T^*}(\varepsilon^*)$ on non-dimensional EDR (ε^*) for $T^*=1,2,3,4$ and 5 for wakes generated in NGE. These results are superimposed with the corresponding $\Gamma^*_{T^*}(\varepsilon^*)$ versus ε^* (in black) for the OGE exponential wake decay model.

The NGE curves show that for a given T^*, NGE circulation decay is less sensitive to EDR than the OGE counterpart. Also note that the circulation decay range within the two extreme limits of ε^* are

less than that of OGE. However, the data also showed that at a given ε^*, with increasing T^* the circulation decays are much faster than their OGE counterparts. These trends suggest that, within the range of ε^* examined, environmental turbulence plays a secondary role. Another source of high turbulence is that generated in the near vicinity by the vortex-ground interaction itself, which could be the primary cause for accelerated decay observed within the low to moderate turbulence environment in the dataset. As reported by Burnham and Hallock (2005), under low and moderate ambient turbulence, the turbulence level inside of the vortex flow field near the ground is higher than that of the ambient turbulence existing in the wind.

Note that the T^*_{Max} statistics have the maximum range of 4 to 5 non-dimensional times. However, the circulation values at T*=4 and T*=5 are still above the minimum sensitivity of wake strength measurements from the LIDAR, thereby suggesting that NGE wake demise is more likely driven by an earlier onset of a wake going to a catastrophic state due to instability. Additionally, to insure that the differences in means and medians of the circulation values between the highest and lowest EDR bins are statistically significant, the T-test (for the difference in the means of two independent normally-distributed populations) and the Wilcoxon rank-sum test (on the difference of the medians) were performed. For a significance level α=.01, circulation data for T*=3,4,5 passed the T-test, while data for all values of T^* passed the Wilcoxon test. This indicates that at least for non-dimensional times greater than three, the differences are statistically significant.

5. CONCLUSION AND FUTURE WORK

Analysis of wake and turbulence data collected at IAH for the NGE regime show that the downwind wake age decreases under higher winds. The observation is most likely due to an increase of turbulence (as measured in terms of EDR) under higher wind conditions near the surface. The sonic and ASOS anemometer data collected show that, during the measurement period, EDR increases by about two orders of magnitude when the mean ASOS wind increases from 1 to 14 knots. The similar trends seen in data-derived wake age versus EDR curves and the Sarpkaya model for time to a catastrophic wake state versus EDR suggest that the shorter NGE wake age is due to a faster wake breakup under higher turbulence. This conclusion is further strengthened by the relatively slow dependence of circulation decay on ε^* at a fixed T^*. It should however be kept in mind that, as stated earlier, the range of ε^* investigated does not extend to high turbulence regime, where the ambient turbulence may contribute to the overall decay more significantly. The accelerated NGE circulation decay prior to wake demise suggests that the decay is more likely attributed to the turbulence inside of the vortex flow field. However, the final demise appears to be driven by instability introduced from the ambient turbulence.

Assessing the generality and portability of these results to other sites requires analysis of greater data sets from different airports. A particular interest would be to include data from other airports which would yield a wider range of EDR to be considered. The logical next phase also involves bounding wake age based on atmospheric measurements for the purpose of supporting the safety case for new departure procedures.

6. ACKNOWLEDGEMENT

The support and encouragement from Steven Lang, Jeffery Tittsworth and Edward Johnson of the FAA, and Michael Geyer and Nelson Keeler of the DOT Volpe Center are gratefully acknowledged. The authors also thank Kevin Clark and Khang Nguyen of the DOT Volpe Center, and Leo Jacobs of L3-Communications for their efforts in data collection and the overall maintenance of the test site.

7. REFERENCES

Bryant, W., Lang, S., Tittsworth, J., and Darr, S., “Wake Vortex Avoidance System,” Paper 2007-175, Proceedings of the 1st CEAS European Air and Space Conference – Century Perspectives, September 10-13, Berlin, Germany.

Burnham, D. C., and Hallock, J. N., “Measurements of Wake Vortices Interacting with the Ground,” *Journal of Aircraft*, Vol. 42, No. 5, September-October 2005, pp. 1179-1187.

Dee, F. W., and Nicholas, O. P., “Flight Measurements of Wing-Tip Vortex Motion Near the Ground,” Aeronautical Research Council C.P. No. 1065, January 1968.

Frech, M., "Estimating the Turbulent Energy Dissipation Rate in an Airport Environment," *Boundary-Layer Meteorol*, 2007, pp. 385-393.

Gerz, T., Holzäpfel, F., and Darracq, D., "Commercial Aircraft Wake Vortices," *Progress in Aerospace Sciences*, Vol. 38, 2002, pp. 181-208.

Greene, G. C., "An Approximate Model of Vortex Decay in the Atmosphere," *Journal of Aircraft*, Vol. 23, No. 7, July 1986, pp. 566-573.

Hannon, S. M., Phillips, M. W., Thompson, J. A., and Henderson, S. W., "Pulsed Coherent Lidar Wake Vortex Detection, Tracking and Strength Estimate in Support of AVOSS," NASA First Wake Vortex Dynamic Spacing Workshop – NASA CP-97-206235, 1997, NASA Langley Research Center, Hampton, VA.

Holzäpfel, F., and Steen, Meiko, "Aircraft Wake – Vortex Evolution in Ground Proximity: Analysis and Parameterization," *AIAA Journal*, Vol. 45, No. 1, January 2007, pp. 218-227.

Jackson, P., (ed) "Jane's All the World's Aircraft," Jane's Information Group, Various Volumes.

Köpp, F., "Wake-Vortex Characteristics of Military-Type Aircraft Measured at Airport Oberpfaffenhofen Using the DLR Laser Doppler Anemometer," *Aerospace Science and Technology*, 1999, No. 4, pp. 191-199.

Lang, S., Tittsworth, J., Domino, D., Lunsford, C., Clark, D., Robasky, F., and Lohr, G., "Wake Turbulence Mitigation for Departures from Closely Spaced Parallel Runways: A Research Update," Paper 2007-176, Proceedings of the 1st CEAS European Air and Space Conference – Century Perspectives, September 10-13, Berlin, Germany.

Mackey, S. M., Wang, F. Y., Wassaf, H., and Soares, M., "Comparison Between Arrival and Departure Wake Vortex Statistics Near the Ground," Paper 2007-002, Proceedings of the 1st CEAS European Air and Space Conference – Century Perspectives, September 10-13, Berlin, Germany.

Perras, G. H., and Dasey, T. J., "Turbulence Climatology at Dallas/Ft. Worth (DFW) Airport – Implications for a Departure Wake Vortex Spacing System," MIT Lincoln Laboratory Project Report NASA/L-4, November 2000.

Proctor, F. H., Hamilton, D. W., and Han, J., "Wake Vortex Transport and Decay in Ground Effect: Vortex Linking with the Ground," AIAA Paper 2000-0757, Reno, NV., January 2000.

Robins, R. E., and Delisi, D. P., "Algorithm for Prediction of Trailing Vortex Evolution," *Journal of Aircraft*, Vol. 38, No. 5, September-October, 2001, pp. 911-917.

Sarpkaya, T., Robins, R. E., and Delisi, D. P., "Wake-Vortex Eddy-Dissipation Model Predictions Compared with Observations," *Journal of Aircraft*, Vol. 38, No. 4, July-August 2001, pp. 687-692.

Spalart, P. R., Strelets, M.-Kh., Travin, A. K., and Shur, M. L., "Modeling the Interaction of a Vortex Pair with the Ground," *Fluid Dynamics*, Vol. 36, No. 6, 2001, pp. 899-908.